

Inhomogeneous Big-Bang Nucleosynthesis in Light of Recent Observations

K. Kainulainen^{a,*}, H. Kurki-Suonio^{b,†}, and E. Sihvola^{c,‡}

^a*NORDITA, Blegdamsvej 17, DK-2100, Copenhagen Ø, Denmark*

^b*Helsinki Institute of Physics, P.O.Box 9, FIN-00014 University of Helsinki, Finland*

^c*Department of Physics, P.O.Box 9, FIN-00014 University of Helsinki, Finland*

(July 9, 1998)

We consider inhomogeneous big bang nucleosynthesis in light of the present observational situation. Different observations of ^4He and D disagree with each other, and depending on which set of observations one uses, the estimated primordial ^4He corresponds to a lower baryon density in standard big bang nucleosynthesis than what one gets from deuterium. Recent Kamiokande results rule out a favorite particle physics solution to this tension between ^4He and D. Inhomogeneous nucleosynthesis can alleviate this tension, but the more likely solution is systematics in the observations. The upper limit to Ω_b from inhomogeneous nucleosynthesis is higher than in standard nucleosynthesis, given that the distance scale of the inhomogeneity is near the optimal value, which maximizes effects of neutron diffusion. Possible sources of baryon inhomogeneity include the QCD and electroweak phase transitions. The distance scale of the inhomogeneities arising from the electroweak transition is too small for them to have a large effect on nucleosynthesis, but the effect may still be larger than some of the other small corrections recently incorporated to SBBN codes.

PACS numbers: 98.80.Cq, 98.80.Ft

I. INTRODUCTION

Standard big bang nucleosynthesis [1–4] (SBBN) predicts the primordial abundances of D, ^3He , ^4He , and ^7Li as a function of a single parameter, the baryon-to-photon ratio $\eta \equiv n_b/n_\gamma$, which is related to the baryonic mass-density parameter $\Omega_b \equiv 8\pi G \rho_{b0}/3H_0^2$ by

$$\Omega_b h^2 = 3.70 \times 10^{-3} \eta_{10}, \quad (1)$$

where $\eta_{10} \equiv 10^{10} \eta$ and $h \equiv H_0/100 \text{km s}^{-1} \text{Mpc}^{-1}$. The observed abundances of these isotopes are in a rough agreement with the SBBN predictions [5] for a range of η_{10} , which is compatible with other cosmological bounds on the amount of baryonic matter in the universe. In principle, comparing SBBN predictions with primordial abundances extrapolated from observations pins down the precise value of η_{10} . A few years ago the standard result was $\eta_{10} \sim 3\text{--}4$ [3,4], but even much tighter constraints were published (e.g., $2.69 \leq \eta_{10} \leq 3.12$ [6]). Recently the situation has become more complicated, and it seems that such precise determinations were premature.

Since the discovery of the τ lepton, implying three flavours of light neutrinos, there has been tension between ^4He and D in SBBN [7,8]. Olive *et al.* [9] (OSS97)

have reviewed the ^4He observations and their best estimate is

$$Y_p = 0.230 \pm 0.003. \quad (2)$$

This corresponds to $\eta_{10} = 1.4 \pm 0.3$ and hence to primordial D/H $\sim 2\text{--}3 \times 10^{-4}$ in SBBN, whereas the present D/H in the ISM is [10] only 1.5×10^{-5} . Most models of galactic chemical evolution have difficulty explaining this much deuterium abstraction [11], and prefer a much lower primordial D/H and thus a higher baryon density, $\eta_{10} \sim 5$.

The conventional way to deal with this tension has been to compromise by settling on an intermediate η_{10} which is preferred neither by ^4He nor by D/H but is considered acceptable to both. This however, leads to an artificially high precision in the η_{10} determination, because while the individual ranges in η_{10} accepted by ^4He and D/H are wide, their overlap is narrow. Tension increased when data was subjected to more thorough formal statistical analysis, culminating in a claim of a “crisis” in SBBN, by Steigman *et al.* [12], who concluded that given the existing data the overlap is in fact nonexistent.

In the context of SBBN the resolution of this crisis requires either a revision of the picture of the galactic chemical evolution [13], so that much more deuterium abstraction can be accommodated [14], or a large systematic error in the Y_p determination from the observations [5,15,16]. Indeed, based on a number of new ^4He observations, Izotov and Thuan [17] have claimed a significantly higher Y_p than OSS97:

$$Y_p = 0.244 \pm 0.002. \quad (3)$$

Whether this new value is to be accepted as such over the old OSS97 value is yet unclear, since several sources of poorly known systematic effects are expected to contribute to the discrepancy [18].

Interestingly, some particle physics solutions based on a massive decaying tau neutrino [19] can now be ruled out using the recent results from Kamiokande [20]. The directional dependence in the upward going muon neutrino deficiency seen in the Super Kamiokande experiment is a strong implication that the muon neutrinos undergo oscillations while traversing through the earth. This implies that ν_μ mixes with either a tau neutrino or a new sterile neutrino with a mass splitting of about $\delta m^2 \sim 10^{-3} \text{eV}^2$ and with an almost maximal mixing angle. If this mixing is between ν_μ and ν_τ , then ν_τ is obviously light so that the scenarios based on heavy ν_τ

decaying into ν_μ and some scalar particle [19] are immediately ruled out. Suppose then that the atmospheric anomaly is due to mixing between ν_μ and some sterile neutrino. Now ν_τ can be heavy and having it decay away to muon neutrino and a scalar state prior nucleosynthesis could alleviate the tension somewhat. The effect is roughly equivalent to having about a half a neutrino degree of freedom worth less energy density in the universe [19] (less energy density leads to slower expansion, and hence later decoupling of n/p -ratio). However, the sterile state with the requested mixing parameters is brought into full thermal equilibrium due to oscillation and quantum damping prior to nucleosynthesis [21], overcoming the alleviating effect discussed above and making the tension even worse. The only possibility to alleviate the tension is that $m_{\nu_\tau} \lesssim 1$ MeV and ν_τ decays into an *electron neutrino* in the short interval after the electron neutrino freezeout but prior the onset of nucleosynthesis. In this case the excess (almost thermal) electron neutrinos can significantly increase the weak interaction rates keeping the n/p -ratio in equilibrium longer and hence leading to much less helium being produced [22,23]. Bringing the sterile neutrino into equilibrium makes also this solution less effective, but is not strong enough to rule out the possibility entirely [23,24].

The chemical evolution of D and ^4He is particularly simple: ^4He increases with time, whereas D decreases. In contradistinction, ^3He and ^7Li are both produced and destroyed during galactic chemical evolution. Thus it is much more difficult to make reliable claims of their primordial abundances based on present abundances. Observed ^3He abundances [25] in particular vary a lot within the galaxy and ^3He observations are useful for constraining BBN only when combined with D and chemical evolution models.

For ^7Li there is a very impressive plateau [26] of abundances in PopII stars with surface temperatures $T = 5800\text{--}6400$ K. The observed value is [27,28]

$$\log_{10}(^7\text{Li}/\text{H}) = -9.75 \pm 0.10. \quad (4)$$

The universality of this abundance suggests that it is closely related to the primordial abundance. There may have been some depletion, i.e., some of the surface ^7Li has been destroyed by the star. Therefore the primordial abundance should be larger by some depletion factor D_7 . Pinsonneault *et al.* [28] estimate $D_7 = 0.2\text{--}0.4$ dex. This corresponds to a primordial

$$\log_{10}(^7\text{Li}/\text{H})_p = -9.45 \pm 0.20. \quad (5)$$

However, Vauclair and Charbonnel [29] give a lower estimate

$$\log_{10}(^7\text{Li}/\text{H})_p = -9.65 \pm 0.10. \quad (6)$$

These estimates for lithium are compatible with either a low, $\eta_{10} \sim 1.5$, or a high, $\eta_{10} \sim 4\text{--}6$ baryon density, but disfavor a compromise value $\eta_{10} \sim 2.5\text{--}3$.

A promising new method with the potential to resolve this η dicotomy is the observation of deuterium in clouds at high redshifts by its absorption of quasar light [30]. Some of these clouds are so far away, that when the observed light passed through them, the universe was a mere one-tenth of its present age; thus the matter in these clouds and therefore the observed deuterium abundance should be close to primordial. Unfortunately, at present we only have a small number of such D/H measurements, and even the existing ones are still controversial. Burles and Tytler [31] obtain from their two best observations

$$\text{D/H} = 3.4 \pm 0.3 \times 10^{-5}, \quad (7)$$

which corresponds to $\eta_{10} = 5.1 \pm 0.3$ in SBBN. This is in contradiction with the OSS97 estimate $Y_p \sim 0.23$. However, the analysis of Burles and Tytler has been debated [32] and one observation by HST [33] from an absorption cloud at $z = 0.7$ appears to give a *high* value of $\text{D/H} \sim 2 \times 10^{-4}$.

Thus the observational situation remains unclear. If we suppose that some of the determinations of primordial abundances are correct, but we do not know which, we are led to an SBBN range

$$\eta_{10} \sim 1.5\text{--}6. \quad (8)$$

One can also try to determine the universal baryon density by other means, discarding nucleosynthesis considerations [34]. Determinations of this kind are rather uncertain at present, but tend to favor the larger values of η .

In conclusion, there is an unsettled disagreement between different observations in the context of SBBN. While the problem may lie with the observations, or in the determination of primordial abundances from them, another possibility is, that the primordial abundances indeed do not correspond to the same η in SBBN, so that it needs to be modified. In this paper we study the possibility of inhomogenous big bang nucleosynthesis (IBBN) in light of the present observational situation. In section II we discuss the generic mechanisms known to produce inhomogeneities in the baryon distribution and the significance of the distance scale of the inhomogeneity. We describe our numerical calculations in section III and give our results in section IV. Section V contains our conclusions.

II. INHOMOGENEOUS NUCLEOSYNTHESIS

In SBBN we assume baryonic matter was homogeneously distributed during nucleosynthesis, but actually we do not know whether this was the case. If the inhomogeneity was of sufficiently small scale, diffusion would have homogenized the matter distribution before the formation of the cosmic microwave background leaving no directly observable trace today.

A. Generating the inhomogeneity

Various phase transitions which took place before nucleosynthesis in the early universe were capable of producing large-amplitude small-scale fluctuations in the baryon number density: in particular the electroweak (EW) transition at $T \sim 100$ GeV and $t \sim 10^{-11}$ s and the QCD transition at $T \sim 150$ MeV and $t \sim 10^{-5}$ s.

IBBN was studied extensively in the late 1980's, when it was realized that a first-order QCD phase transition in the early universe could produce the kind of inhomogeneity which would affect BBN [35–44]. At first [35,37,39] it seemed possible to accommodate much larger values of η_{10} , even $\Omega_b = 1$, but more detailed calculations [38,40,42,45–47] showed that the upper bound to η_{10} was in fact much less increased.

The original mechanism relying on chemical pressure [48], operative in the QCD transition, leads to a geometry where localized clumps of high density are surrounded by large voids of low baryon density [49–52]. The details of the QCD transition are poorly known and both the amplitude and the size of the inhomogeneities can vary significantly; the size of course is bounded by the horizon at the QCD transition, which is about 2×10^6 m (at $T = 1$ MeV) = 0.4 pc (today).

Also the electroweak phase transition (EWPT) generically produces inhomogeneities, and possibly with large density contrasts. This assumes of course that the baryons we see around us today, were generated during the electroweak phase transition [53]. Some scenarios [54,55] may even give rise to regions of antibaryons mixed with the overall baryonic excess, leading to the interesting possibility of nucleosynthesis in the presence of antibaryons [56,57]. The generic feature leading to the formation of inhomogeneities in the more standard scenarios is the strong dependence of the baryoproduction rate on the bubble wall velocity in the so called "charge transport mechanism" [58–60], coupled with the characteristic changes in the velocity of the bubble walls during the transition [61]. For thin walls one finds a local baryoproduction rate

$$B(x) \approx c/v_w(x). \quad (9)$$

The velocity dependence of the local baryoproduction rate due to the "classical chiral force" mechanism [62,63], operative in the limit of wide walls, is much weaker [64]. However, the generic geometry of inhomogeneities arising from EWPT is quite opposite to the QCD case; voids of low density surrounded by walls of high density.

After nucleation bubble walls quickly accelerate to a terminal velocity $v_w \sim 0.1\text{--}0.5c$, whose exact value depends on the parameters of the phase transition, like the latent heat released, the surface tension and the frictional forces effected on the bubble wall by the ambient plasma [65,66]. After some time (we are only considering deflagration bubbles here), the shock waves preceding phase transition fronts collide reheating the unbroken

phase plasma back to the critical temperature. As a result the pressure forces driving the bubble expansion are reduced, and, were it not for the general expansion of the universe, the walls would become to a complete stop. Due to Hubble expansion the walls can still continue expanding, but now with a greatly reduced speed, typically $v_w \sim \mathcal{O}(\text{few}) \times 10^{-3}c$ [66]. These velocity scales and the rate (9) indicate that the maximal density contrast possibly generated by the EW mechanism is about ~ 100 .

The typical size of the voids in this "beer foam" geometry is some fraction of the horizon at the EW transition, $\ell_H = 3 \times 10^3$ m (at 1 MeV) = 6×10^{-4} pc (today). A nucleation calculation, which ignores the thermodynamics of the bubble interactions, typically gives for the size of bubbles at the coalescence only $\ell_b \sim 10^{-3}\ell_H$ [66–68]. However, due to reheating the firstly nucleated bubbles may inhibit the growth of bubbles formed only slightly later, increasing perhaps significantly the size of the largest structures as compared with the simplest nucleation estimate. Also in extended scenarios including magnetic fields [55], the size of a single bubble can reach the horizon scale. We then consider the inhomogeneity size a free parameter, with values $r \sim 10^{-3} \text{--} 1\ell_H$.

B. Distance scales

Both the EW and the QCD transition appear capable of producing high initial density contrasts. In both cases the density fluctuations would be non-gaussian, consisting of high- and low-density regions. The pattern would not be regular, but it would have a characteristic distance scale. The inhomogeneity can be described by the typical geometric shape of these regions and the following three parameters: 1) typical distance scale r , 2) typical density contrast $R \equiv \eta_{\text{high}}/\eta_{\text{low}}$, and 3) the volume fraction f_v of the high-density regions.

The distance scale r is especially important. An inhomogeneity can have a large effect on nucleosynthesis only if the distance scale is comparable to the neutron diffusion length d_n during nucleosynthesis. If the distance scale is too small, $r \ll d_n(500 \text{ keV}) \sim 200$ m (at 1 MeV) $\sim 4 \times 10^{-5}$ pc (today), the inhomogeneity is erased before nucleosynthesis, because before the weak freeze-out protons and neutrons are constantly converted to each other by weak reactions, and the diffusion thus evens out both the proton and the neutron density.

If the distance scale is large, $r \gg d_n(10 \text{ keV}) \sim 500$ km (at 1 MeV) ~ 0.1 pc (today), diffusion does not occur until nucleosynthesis is completed. In this "ordinary inhomogeneity" scenario, the high- and low-density regions undergo independent standard BBN with η_{high} and η_{low} and the matter is mixed afterwards to have the average baryon-to-photon ratio η . Leonard and Scherrer [69] have shown that this kind of inhomogeneity cannot increase the upper limit to η , since the inhomogeneity

raises ${}^4\text{He}$ yields. Arbitrarily low η can be made acceptable with these models, however.

An intermediate distance scale, $d_n(500 \text{ keV}) < r < d_n(10 \text{ keV})$ leads to nucleosynthesis with inhomogeneous neutron-to-proton ratio. The strongest effect occurs if $n/p \gg 1$ in some region, because in this region neutrons are left over from ${}^4\text{He}$ synthesis. This can be induced in the low-density region if $f_v R \gg (n/p)^{-1}$ before diffusion. QCD-scale inhomogeneities could be [51] of the scale required, although QCD lattice calculations [70] favor values below the short end of this range. For the EW case this range corresponds to a fluctuation scale $r \gtrsim 0.1\ell_H$ during the transition.

There may be other possible sources of baryon inhomogeneity in addition to the EW and QCD phase transitions. Moreover, there is a considerable uncertainty regarding the parameters r , R and f_v from each transition. Therefore it is natural to treat the two questions separately: 1) Are there IBBN parameter regions where IBBN agrees with observations equally well or better than SBBN? 2) Could the EW or QCD phase transitions produce inhomogeneity in this parameter region?

III. COMPUTATIONS

The IBBN code used for this paper is based on the code used in [43] and the nuclear reaction rates have been updated according to [4]. In the ${}^4\text{He}$ yield we take into account the various corrections to the weak reaction rates [8,6,71]. Theoretical uncertainty in abundance yields due to uncertainty in nuclear reaction rates is usually small compared to observational uncertainties. An exception is the ${}^7\text{Li}$ yield for which one standard deviation is 0.07–0.10 dex upwards and 0.11–0.19 downwards [4]. We take this into account when obtaining limits on η from ${}^7\text{Li}$ deduced from observations, by further relaxing the upper limit to ${}^7\text{Li}$ by 0.15 dex and the lower limit by 0.10 dex. Proton diffusion is included according to [72]. The convergence of the code has been improved by combining the nuclear reaction and diffusion steps into a single step, which reduces the number of time steps needed for accurate results.

We assume spherical symmetry and use a nonuniform radial grid of 64 zones representing a sphere with comoving radius r , with reflective boundary conditions both at the center and at r . This setup allows us to model both geometries discussed above: assuming centrally condensed density describes the QCD-type and spherical shells of high density describe the EW-type geometry. The volume fraction covered by the high density region in each geometry is

$$f_v = f_r^3 \quad (\text{centrally condensed}), \quad (10)$$

$$f_v = 1 - (1 - f_r)^3 \quad (\text{spherical shell}), \quad (11)$$

where f_r denotes the fraction of the radius covered by the high-density region. Given the geometry, the model

is specified by four parameters: r , f_v , R described above, and the average baryon-to-photon ratio η . The numerical value for η always refers to the present value, i.e., after e^+e^- -annihilation.

Note that these inhomogeneities are in baryon number only. At nucleosynthesis time, the energy density is dominated by radiation by a factor of at least 10^5 . The density of baryon number can hence be strongly inhomogeneous without a noticeable dynamic effect, and the main process through which the inhomogeneity evolves after the phase transition is diffusion [35,72,46].

The effect of neutron diffusion is to reduce ${}^4\text{He}$ and ${}^7\text{Li}$ yields, and to increase D and ${}^3\text{He}$ yields. All these changes are in the direction of favoring a larger η . However, diffusion has to compete with the ordinary inhomogeneity effect which for ${}^4\text{He}$, ${}^7\text{Li}$, and ${}^3\text{He}$ is the opposite, increasing ${}^4\text{He}$ and ${}^7\text{Li}$ and reducing ${}^3\text{He}$. For D this latter effect depends on the average η . For small η , D is reduced, and for large η D is increased.

The most dramatic effect is obtained when the neutron diffusion out of the high-density region leads to a large excess of neutrons in the low-density region. This requires a density contrast

$$R \gg \left(\frac{p}{n}\right)_0 \frac{1}{f_v}, \quad (12)$$

where $(p/n)_0 \sim 7$ is the SBBN proton/neutron ratio at the onset of nucleosynthesis. Increasing R leads to a stronger effect, but the increase soon saturates. Indeed, for large R almost all of the nuclear matter already is in the high-density region, while almost no matter remains in the low density regions:

$$\eta_{\text{high}} = \frac{R\eta}{f_v R + 1 - f_v} \xrightarrow{R \rightarrow \infty} \frac{\eta}{f_v}, \quad (13)$$

$$\eta_{\text{low}} = \frac{\eta}{f_v R + 1 - f_v} \sim \frac{\eta}{f_v R} \xrightarrow{R \rightarrow \infty} 0. \quad (14)$$

R	f_r	f_v	$f_v R$
Centrally condensed (c.c.)			
283	$1/\sqrt{2}$	0.3536	100
800	$1/2$	0.125	100
2263	$1/2\sqrt{2}$	0.0442	100
6400	$1/4$	0.0156	100
51200	$1/8$	0.0020	100
Spherical shell (s.s.)			
1000	$1/4$	0.5781	578
1000	$1/8$	0.3301	330
1000	$1/16$	0.1760	176
1000	$1/32$	0.0909	91
1000	$1/64$	0.0461	46
1000	$1/128$	0.0233	23

TABLE I. The different geometries studied. R is the density contrast between the high and low density, f_r is the high-density fraction of the grid radius, and f_v is the corresponding volume fraction.

The effect of further increasing R , beyond, say $R = 100/f_v$, just leads to a further reduction of matter density in the low-density region and has essentially no effect on nuclear yields. An exception to this may be D, since the D yield drops so fast with increasing η , that a significant part of the D yield may still come from the low-density region, giving rise to sensitivity to a reduction of η_{low} and hence to R .

In most cases we chose to run with large enough R to have close to this maximal effect. This leaves us with three parameters f_v, η, r . We did runs with 11 different values of f_v altogether (Table I).

For the runs with spherical shell geometry, we kept $R = 1000$ constant. For the centrally condensed geometry some of the volume fractions were so small, that a larger R was needed to get the large inhomogeneity effect. For the centrally condensed runs we kept the product $f_v R = 100$ constant instead.

IV. RESULTS

It has been customary in IBBN studies [40,44,45,47] to plot the regions in the (η, r) -plane allowed by different observational constraints. Since the observational situation has become rather less clear recently, we present the results first as abundance contours for a given geometry and f_v , so different constraints can then be applied afterwards. For ${}^4\text{He}$ we plot the mass fraction Y_p , for D and ${}^7\text{Li}$ we plot the number ratios D/H and ${}^7\text{Li}/\text{H}$. To save space, the less interesting ${}^3\text{He}$ is not shown.

In Fig. 1 we show the results for the spherical shell (s.s.) geometry with $R = 1000$ and $f_r = 1/16$. It is clear that at the distance scales attainable in the EW transition (indicated by the lower horizontal dashed line in the figure) the IBBN results do not significantly differ from SBBN results; the observational uncertainties are certainly much larger. However, even with scales as small as $r \sim 0.05\ell_H$, the effect of inhomogeneity (see Fig. 2) can be larger than certain small corrections recently included into the SBBN computations [71].

Now we take a somewhat different point of view and consider a broader range of density contrasts and distance scales than can be produced in the electroweak phase transition. In Figs. 3 and 4 we present the results for the centrally condensed (c.c.) runs with $f_r = 1/2$ and $f_r = 1/4$. The results from other runs described in Table I are qualitatively similar.

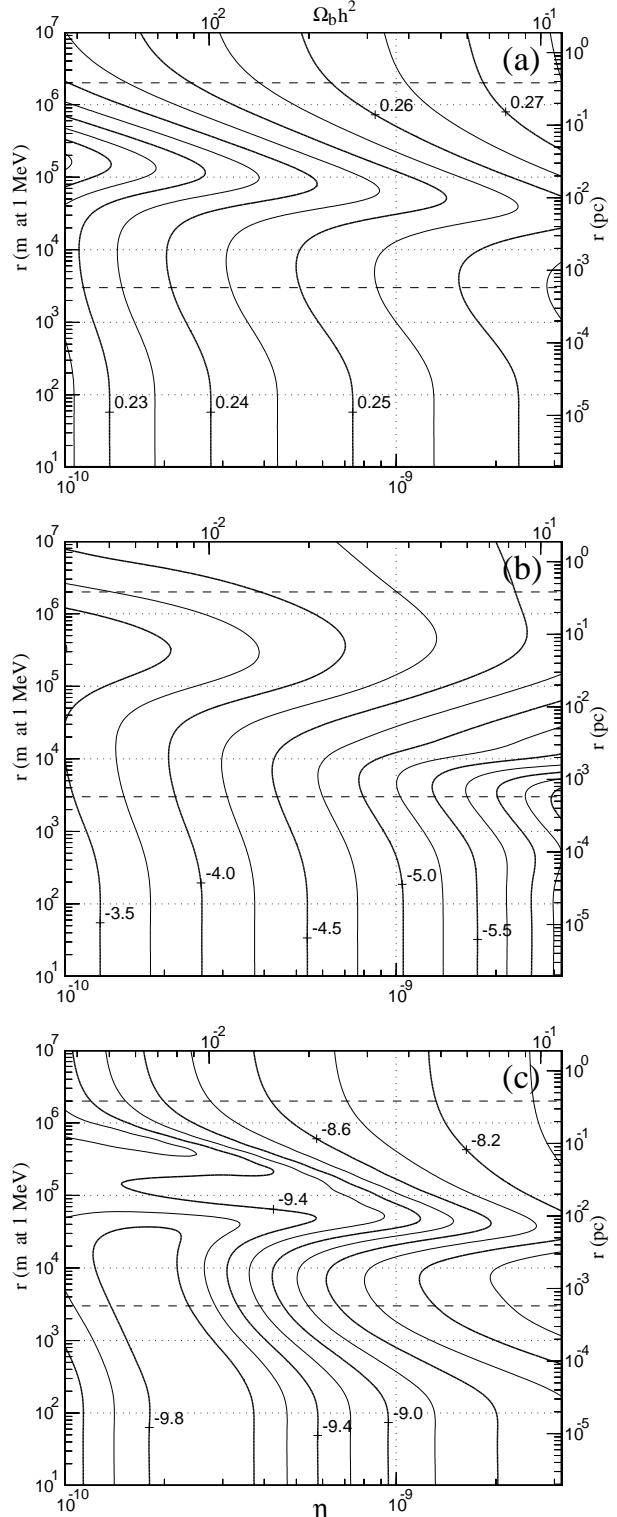


FIG. 1. The ${}^4\text{He}$, D, and ${}^7\text{Li}$ yields from inhomogeneous nucleosynthesis runs with the spherical shell geometry, with $R = 1000$ and $f_r = 1/16$ ($f_v = 0.176$). The contours of (a) Y_p , (b) $\log_{10} \text{D/H}$, and (c) $\log_{10} {}^7\text{Li}/\text{H}$ are plotted as a function of the average baryon-to-photon ratio η and the distance scale r of the inhomogeneity. The two horizontal dashed lines denote the horizon scale ℓ_H at the QCD (upper) and EW (lower) phase transitions.

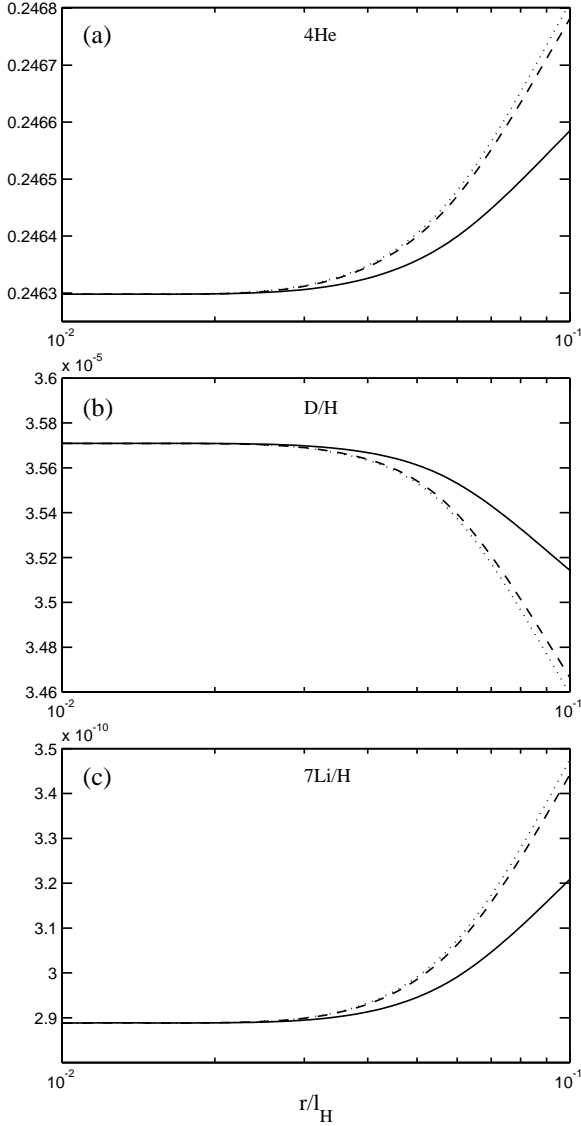


FIG. 2. Effects of small scale inhomogeneity on the isotope yields. This figure is for the spherical shell geometry appropriate for the EW transition, and for $f_v = 0.3301$ and $\eta_{10} = 5$. The three lines correspond to $R = 10$ (solid), 100 (dashed), and 1000 (dotted) (or $f_v R = 3.3, 33, 333$), showing how the effect saturates for large R , so that there is little difference between $R = 100$ and $R = 1000$. The horizontal axis gives the ratio of the distance scale to the EWPT horizon.

A. Optimum scales

How much ^4He is produced depends on the number of neutrons available. The yield is minimized at an optimum distance scale $r_{\text{opt}} \sim 10^4 - 10^5$ m, where a maximal number of neutrons diffuse out from the high-density region (where most of the ^4He is produced), but not too many of them diffuse back when the nucleosynthesis in the high-density region starts consuming free neutrons, and the direction of the neutron diffusion reverses. D

yields are maximized at scales somewhat larger than r_{opt} , in particular for large η , because of the strong ordinary inhomogeneity effect. Situation is more complicated with the ^7Li yields, but they tend to be minimized at $r \lesssim r_{\text{opt}}$.

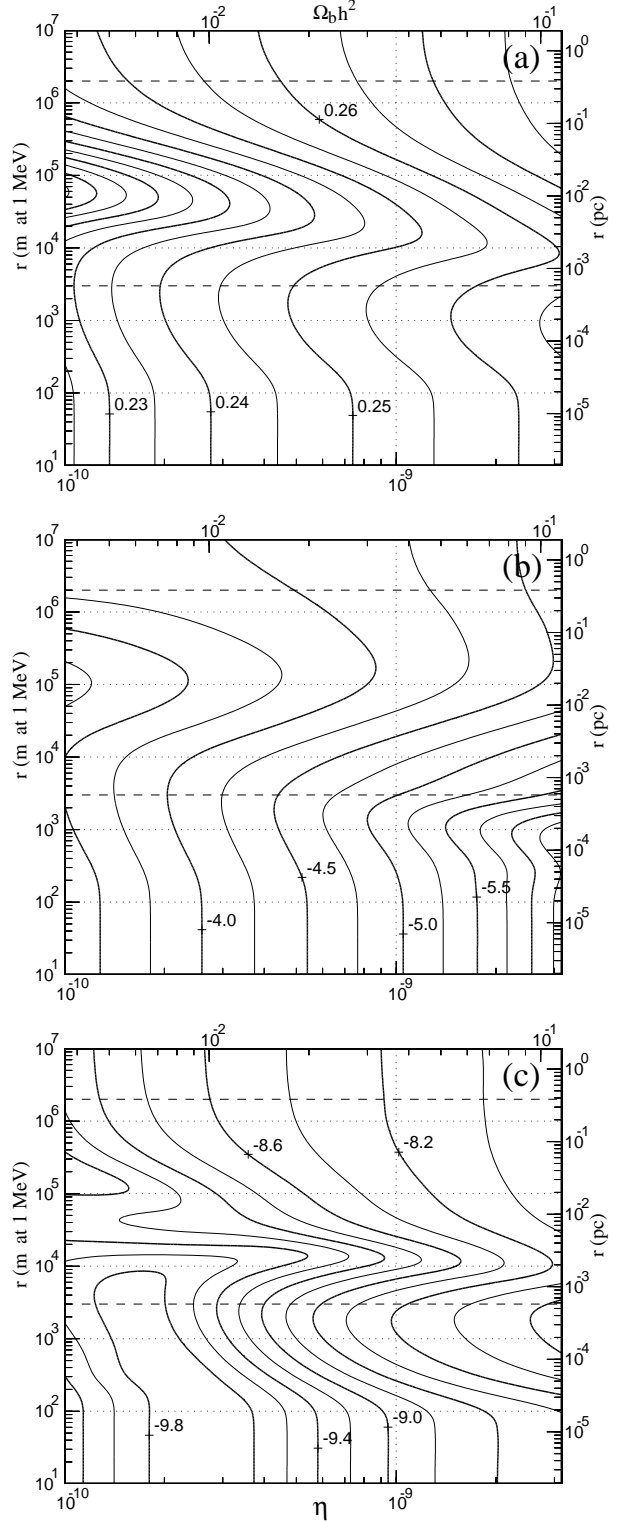


FIG. 3. Same as Fig. 1, but for the centrally condensed geometry with $R = 800$ and $f_r = 1/2$ ($f_v = 0.125$).

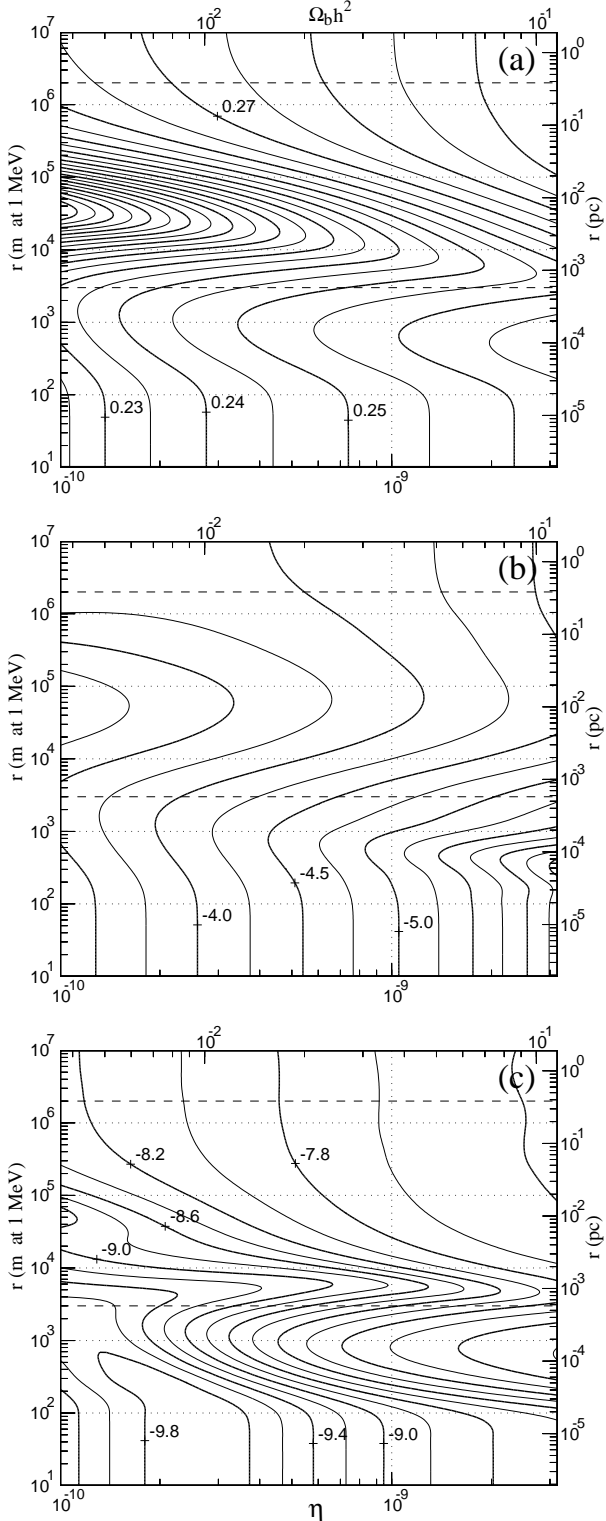


FIG. 4. Same as Fig. 1, but for the centrally condensed geometry with $R = 6400$ and $f_r = 1/4$ ($f_v = 0.0156$).

We find that r_{opt} goes down with increasing η , roughly as $\eta^{-2/3}$. Also, the s.s. geometry gives a larger optimum scale than does the c.c. geometry with the same f_v , and the dependence on f_v is different with different geometries: for centrally condensed spheres r_{opt} goes down with

decreasing f_v , whereas for spherical shells it increases with decreasing f_v .

It is possible to derive the parametric dependence of r_{opt} on η and f_v analytically. Consider the diffusion of neutrons after the weak freeze-out but before the start of nucleosynthesis. The flux of neutrons into the low-density region is proportional to the neutron diffusion coefficient D , to the surface area A of the boundary, and to the gradient of the neutron density at the boundary, roughly $(n_{\text{high}} - n_{\text{low}})/\sqrt{Dt}$. Here \sqrt{Dt} is the diffusion length of neutrons, and n_{high} and n_{low} are the average neutron densities in the high- and low-density regions, respectively. n_{high} decreases as

$$V \frac{\partial n_{\text{high}}}{\partial t} \sim -AD \frac{n_{\text{high}} - n_{\text{low}}}{\sqrt{Dt}} \quad (15)$$

where V is the volume of the high-density region. If we ignore nuclear reactions and weak interactions, we can integrate out Eq. (15). Remembering that $f_v n_{\text{high}} + (1 - f_v) n_{\text{low}} = n_{\text{mean}}$ one readily finds that the density contrast vanishes exponentially due to diffusion:

$$n_{\text{high}} - n_{\text{low}} \sim \exp\left(-\frac{A}{V} \frac{\sqrt{Dt}}{(1 - f_v)}\right). \quad (16)$$

The optimum scale corresponds to

$$\frac{A}{V} \frac{\sqrt{Dt_{\text{ns}}}}{(1 - f_v)} \sim 1 \quad (17)$$

where t_{ns} is the starting time of nucleosynthesis. At scales larger than the optimum scale, the neutrons have not diffused out effectively before the synthesis of ${}^4\text{He}$ begins. On the other hand, making the scale smaller than the optimum scale does not significantly increase the number of neutrons diffusing out, but makes the back-diffusion at later times more effective.

Now it is easy to see why the optimum scales are smaller for condensed spheres. For the same f_v , the surface-to-volume ratio A/V is smaller for condensed spheres than for shell geometry, which makes the out-diffusion less effective and optimum scales smaller.

The efficiency of the out-diffusion also depends significantly on the volume of the low-density region (term $(1 - f_v)$ in the denominator of Eq. (17)). If f_v is large, n_{low} increases rapidly, bringing the diffusion to end sooner than in the case of small f_v .

The η -dependence of the optimum scale is through the dependence on the diffusion length. The diffusion at the boundary is controlled by the smaller diffusion coefficient of the high-density region. The diffusion is dominated by scattering on protons, $D_{np} < D_{ne}$. After electron-positron annihilation the diffusion constant depends on the proton density and temperature as

$$D_n \simeq D_{np} \propto \frac{1}{\eta_{\text{high}} T^{5/2}} \approx \frac{f_v}{\eta T^{5/2}}. \quad (18)$$

The early universe expands as $t \propto 1/T^2$. The diffusion length at the beginning of nucleosynthesis should go as

$$\sqrt{Dt_{\text{ns}}} \propto \eta_{\text{high}}^{-1/2} T_{\text{ns}}^{-9/4} \quad (19)$$

The starting temperature T_{ns} of nucleosynthesis depends on η_{high} : in higher density nucleosynthesis begins earlier. The dependence in the range $\eta_{\text{high}} = 10^{-10} \dots 10^{-8}$ is $T_{\text{ns}} \propto \eta_{\text{high}}^{\gamma}$, $\gamma = 0.07 \dots 0.1$. The diffusion length should depend on η_{high} as

$$\sqrt{Dt_{\text{ns}}} \propto n_{\text{high}}^{-1/2-9\gamma/4} = n_{\text{high}}^{-\alpha}, \quad (20)$$

where $\alpha = 0.65 - 0.73 \sim 2/3$, so that for the optimum scale

$$(1 - f_v) \frac{V}{A} \propto \eta_{\text{high}}^{-2/3}. \quad (21)$$

The surface-to-volume ratio of the high-density region is

$$\frac{A}{V} = \frac{3}{f_v^{1/3} r} \quad (\text{c.c.}) \quad (22)$$

$$\frac{A}{V} = \frac{3(1 - f_v)^{2/3}}{r f_v} \quad (\text{s.s.}).$$

Combining equations (21) and (22) we find the observed behaviour for the optimum scale

$$r_{\text{opt}} \propto \frac{f_v^{1/3}}{(1 - f_v)} \eta^{-2/3} \quad (\text{c.c.}) \quad (23)$$

$$r_{\text{opt}} \propto \frac{\eta^{-2/3}}{f_v^{1/3} (1 - f_v)^{1/3}} \quad (\text{s.s.}).$$

B. Effects on the different isotopes

^4He . For distance scales near the optimal one ^4He yields are reduced. The range in r where the ^4He yield is below the SBBN value covers 1–1.5 orders of magnitude. For the optimum distance scale a given ^4He yield is obtained for a value of η which can be as much as four times larger than in SBBN. Making f_v smaller causes a deeper reduction in ^4He . For the spherical shell geometry we get the maximum effect at $f_r \sim 1/64$ although this may be due to our keeping R fixed to $R = 1000$. In the centrally condensed runs where we keep $f_v R$ constant instead, the effect keeps getting stronger for smaller f_v .

D. The runs near the optimum scale produce more D than SBBN. At these scales the D contours are pushed towards larger η by about the same amount as the ^4He contours. The maximum effect of the inhomogeneity is however at larger scales. Both D and ^4He consistently allow larger η in IBBN near the optimum distance scales.

^7Li . Neutron diffusion helps to reduce the ^7Li yield, since at late times neutrons are diffusing into the high-density regions and destroying ^7Be there. However, the ordinary inhomogeneity effect is to increase ^7Li yields, and usually this effect wins, but for some cases we get a net reduction.

C. Constraints on η

We now compare our IBBN yields to observational constraints. Since at present there is no agreement about what constraints to use, we consider a number of different sets of constraints.

The most fundamental abundance constraints are the upper limit to primordial ^4He and the lower limit to primordial D/H, obtained directly from observed abundances, since chemical evolution always increases the ^4He abundance and reduces D/H. So, in our first set we conservatively take for ^4He the 2- σ upper limit by Izotov and Thuan [17],

$$Y_p \leq 0.248 \quad (24)$$

and for D/H we use the present ISM abundance [10] as the lower limit,

$$\text{D/H} \geq 1.5 \times 10^{-5}. \quad (25)$$

It turns out that all our IBBN models which satisfy Eq. (24) satisfy Eq. (25) also. In Fig. 5 we have plotted the contour (24) from all the models considered here. In SBBN the constraint (24) gives an upper limit to η , $\eta_{10} \leq 6.3$. We see that, e.g., the centrally condensed IBBN models with $f_r = 1/8$ raise this upper limit to

$$\eta_{10} \leq 19, \quad \text{or} \quad \Omega_b h^2 \leq 0.07. \quad (26)$$

Similar results were obtained for the spherical shell geometry with $f_r = 1/32$ or $1/64$; reaching this upper limit requires the distance scale to be close to optimal in order to maximize the effect on η .

While IBBN raises the upper limit to η from ^4He and D/H by a factor of 2 to 3, upper limits from ^7Li are raised at most by a factor of 1.4, and, if we choose a very tight ^7Li limit, not at all. Thomas *et al.* [45] used $^7\text{Li}/\text{H} < 1.4 \times 10^{-10}$, which gives them an SBBN upper limit $\eta_{10} \leq 3.1$, and this limit was not relaxed at all by IBBN. We confirm that none of our IBBN models raises the upper limit to η from this constraint. However, their upper limit for ^7Li allows essentially no depletion at all.

As our second set we take the case for a high η based on the high- z deuterium value of Burles and Tytler [31]. We use the 2- σ range

$$\text{D/H} = 3.4 \pm 0.6 \times 10^{-5} \quad (27)$$

as our constraint. For ^4He we continue to use the Izotov, Thuan [17] upper limit $Y_p \leq 0.248$ and for ^7Li we use the Pinsonneault *et al.* [28] range

$$\log_{10} (^7\text{Li}/\text{H})_p = -9.45 \pm 0.20, \quad (28)$$

further relaxed by the theoretical uncertainties as discussed in Sec. III. The results for this set are displayed in Fig. 6.

In SBBN these constraints lead to a baryon density in the narrow range $\eta_{10} = 4.6\text{--}5.8$. In IBBN the allowed range is

$$\eta_{10} = 3.9\text{--}8.2 \quad (29)$$

for the centrally condensed geometry and

$$\eta_{10} = 3.7\text{--}10.5 \quad (30)$$

for the spherical shell geometry.

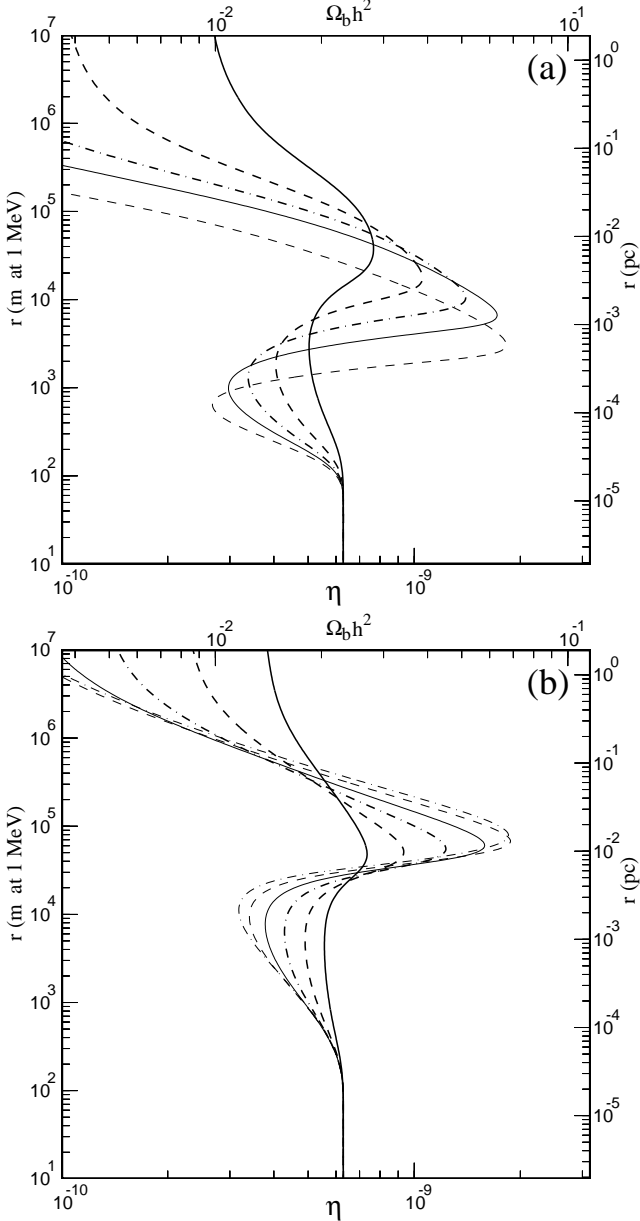


FIG. 5. Conservative upper limit to η from $Y_p \leq 0.248$ and $D/H \geq 1.5 \times 10^{-5}$. The plot (a) is for the c.c. geometry: the thick curves are for $f_r = 1/\sqrt{2}$ (solid), $1/2$ (dashed), $1/2\sqrt{2}$ (dot-dashed), and the thin curves are for $f_r = 1/4$ (solid) and $f_r = 1/8$ (dashed). The plot (b) is for the s.s. geometry: the thick curves are for $f_r = 1/4$ (solid), $1/8$ (dashed), $1/16$ (dot-dashed), and the thin curves are for $f_r = 1/32$ (solid), $1/64$ (dashed), and $1/128$ (dot-dashed). The allowed region is to the left of each curve.

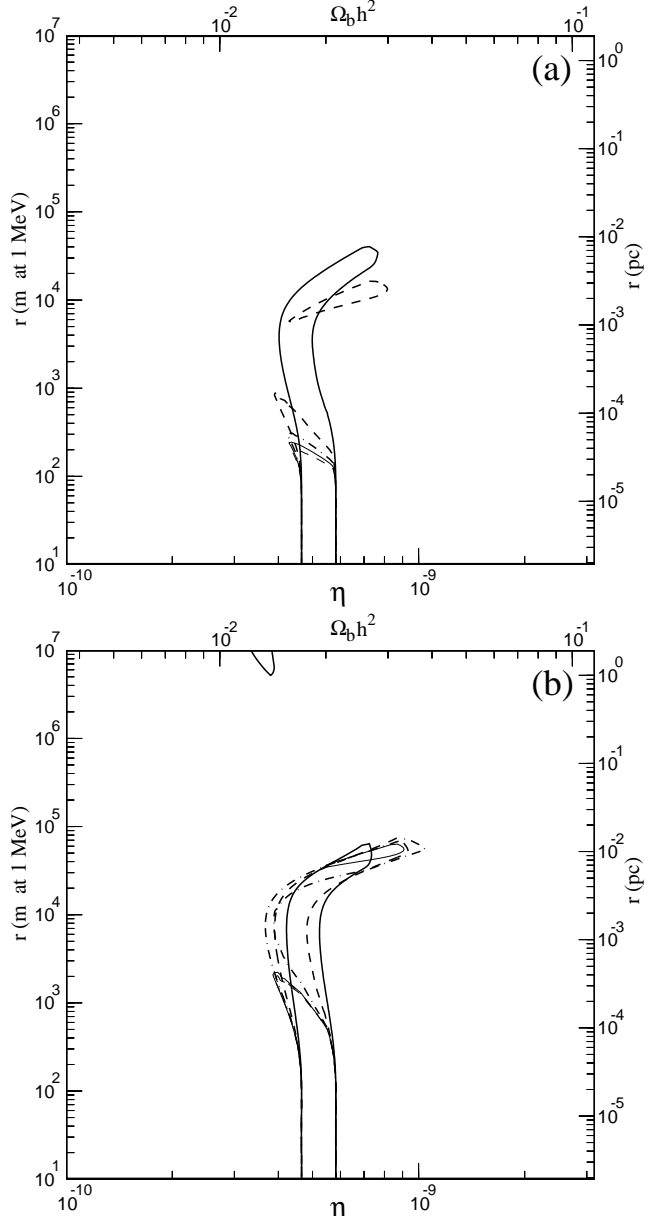


FIG. 6. The regions in the (r, η) -plane allowed by $D/H = 3.4 \pm 0.6 \times 10^{-5}$, $Y_p \leq 0.248$, and $\log_{10} {}^7\text{Li}/H = -9.45 \pm 0.20$. Plot (a) is for the c.c. geometry and plot (b) is for the s.s. geometry. The meaning of the different line styles is the same as in Fig. 5.

In our third set we consider the case for low η in SBBN [13]. (See Fig. 7). The 2- σ OSS97 limits for Y_p

$$0.224 \leq Y_p \leq 0.236, \quad (31)$$

correspond to ${}^7\text{Li}$ near the Spite plateau and a large primordial D. Hence we here use a conservative upper limit to D,

$$D/H \leq 2.5 \times 10^{-4}, \quad (32)$$

and the Vauclair, Charbonnel [29] upper limit for ${}^7\text{Li}$,

$$\log_{10} {}^7\text{Li}/\text{H} \leq -9.55. \quad (33)$$

The results for this set are given in Fig. 7. The SBBN range is $\eta_{10} = 1.5\text{--}2.1$ (lower limit from D/H, upper limit from Y_p). The IBBN upper limits are higher:

$$\eta_{10} \leq 3.6 \text{ (c.c., } f_r = 1/2) \quad (34)$$

$$\eta_{10} \leq 3.8 \text{ (s.s., } f_r = 1/16). \quad (35)$$

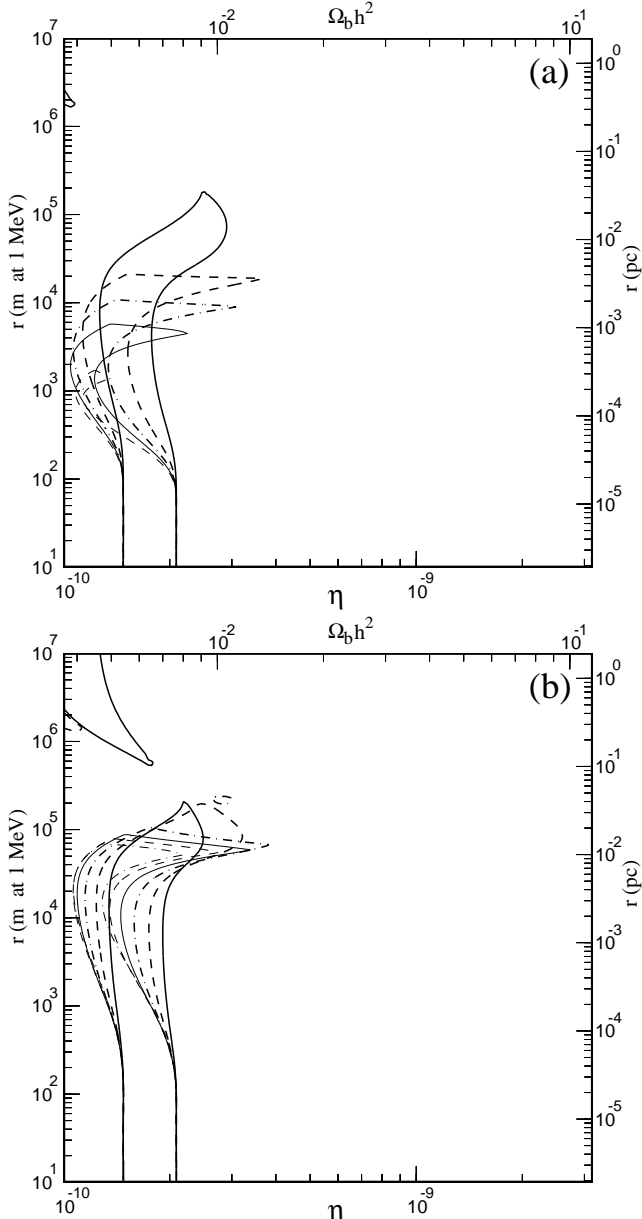


FIG. 7. The case for low η . This figure is similar to Fig. 6, but the constraints used are $Y_p = 0.230 \pm 0.006$, $\text{D}/\text{H} \leq 2.5 \times 10^{-4}$, and $\log_{10} {}^7\text{Li}/\text{H} \leq -9.55$.

We finally demonstrate that IBBN can alleviate the tension between low ${}^4\text{He}$ and low D. If we use the constraints

$$Y_p \leq 0.238, \quad (\text{SBBN } \eta_{10} \leq 2.4) \quad (36)$$

$$\text{D}/\text{H} \leq 10^{-4}, \quad (\text{SBBN } \eta_{10} \geq 2.6) \quad (37)$$

$$\log_{10} {}^7\text{Li}/\text{H} \leq -9.25, \quad (\text{SBBN } \eta_{10} \leq 8.3) \quad (38)$$

no value of η is allowed in SBBN (the “crisis”). However, as is shown in Fig. 8, some IBBN models satisfy these constraints, with $2.6 \leq \eta_{10} \leq 6.0$ (c.c.) or $2.3 \leq \eta_{10} \leq 6.5$ (s.s.), in a narrow (about a factor of two) range of the inhomogeneity distance scale r . This is the “optimum” distance scale, which for these values of η varies between 5 km and 30 km (at 1 MeV) for the centrally condensed geometry. Similar solutions were found with r about 70 km for the spherical shell geometry, proving that the result essentially depends only on the scale and is robust against using different geometries.

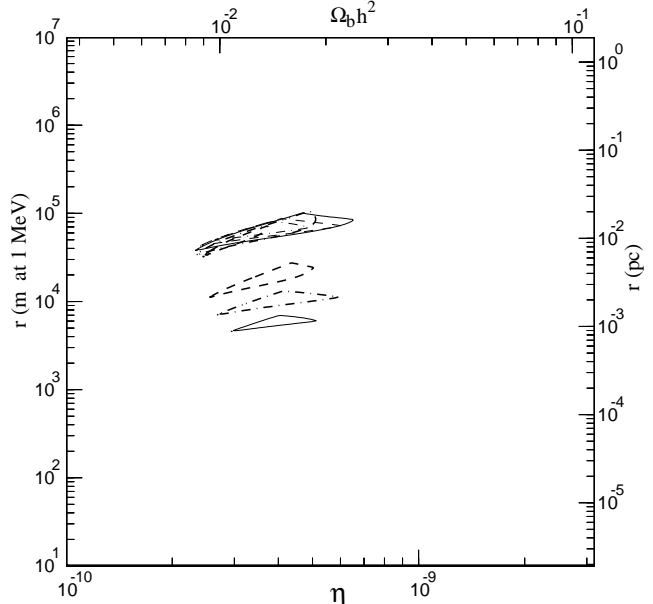


FIG. 8. Alleviating the BBN “crisis”. This figure is similar to Figs. 6 and 7, but the constraints used are $Y_p \leq 0.238$, $\text{D}/\text{H} \leq 10^{-4}$ and ${}^7\text{Li}/\text{H} \leq 10^{-9.25}$. These constraints are incompatible with each other in SBBN, but are compatible in IBBN with the optimal distance scale. The allowed regions for the two geometries are shown in the same plot. The ones for the s.s. geometry are all at the same distance scale and lie on top of each other. For the c.c. geometry we get allowed regions for three of the considered volume fractions, and they lie below the s.s. regions.

V. CONCLUSIONS

In conclusion, we have studied the possibility of inhomogenous nucleosynthesis on the basis of the new observational situation, paying attention to the particular mechanisms capable of producing the inhomogeneities in the very early universe.

First we studied the typical foam like inhomogeneity generated during the electroweak phase transition, which

we modelled by using spherical symmetry with thin shells of high density regions. We find that the scale from the EW transition tends to be too small to cause large deviations from SBBN predictions; that is, the bound on η is not significantly changed. However, the effects on theoretical yields *can be* of equal size or larger than some of the more detailed corrections recently included into the SBBN computations. Due to the genericity of the EW-inhomogeneities these corrections can be claimed to set the scale of accuracy achievable in SBBN computations.

Second we considered the full parameter space of the IBBN models in both centrally condensed (QCD-type) and spherical shell (EW-type) geometries.

To answer the first question posed at the end of Sec. II: IBBN models can satisfy the observational constraints equally well, and for some small region of the parameter space, even better than SBBN. For inhomogeneities with distance scales near the “optimum” scale r_{opt} , where the inhomogeneity effects are maximized, this agreement is obtained for a larger baryon density than in SBBN; precise values depend *intrinsically* on the observational constraints, but the upper limit to η from the upper limit to ${}^4\text{He}$ and from the lower limit to D/H may be raised by a factor of 2–3, whereas upper limits set by the ${}^7\text{Li}/\text{H}$ data are raised less, at most by a factor of 1.4. However, it is not possible ever to get η large enough to make $\Omega_b = 1$. For smaller scales the agreement is obtained for similar or slightly smaller values of η as in SBBN.

Regarding the second question, this optimum distance scale is not only larger than the EWPT horizon, but it is also several orders of magnitude larger than the QCD transition distance scale favoured by QCD lattice calculations of the surface tension and the latent heat. However, the uncertainty in these values is as large as the values themselves so that a much smaller latent heat, leading to a larger distance scale, is still allowed; thus we cannot presently rule out the possibility of reaching the optimum inhomogeneity distance scale in the QCD transition.

There is a region of parameter space, where the tension between ${}^4\text{He}$ and D/H is alleviated compared to SBBN. This takes place if the inhomogeneity distance scale is close to r_{opt} . The effect is however rather small, and for a low deuterium, say $\text{D}/\text{H} \leq 5 \times 10^{-5}$, we cannot accommodate less helium than $Y_p = 0.240$, so IBBN cannot present itself as a solution to a dicotomy in observations. Since we also pointed out that the present Kamiokande result rules out the simplest particle physics solution to possible tension in SBBN, the conclusion, that the problems are probably associated with the observations, is bolstered.

ACKNOWLEDGEMENTS

We thank the Center for Scientific Computing (Finland) for computational resources.

* Email: Kimmo.Kainulainen@nbi.dk
 † Email: Hannu.Kurki-Suonio@helsinki.fi
 ‡ Email: Elina.Sihvola@helsinki.fi

- [1] D.N. Schramm and R.V. Wagoner, Ann. Rev. Nucl. Sci. **27**, 37 (1977); K.A. Olive and D.N. Schramm, in *Review of Particle Physics*, Phys. Rev. D **54**, 109 (1996); B.E.J. Pagel, *Nucleosynthesis and Chemical Evolution of Galaxies*, (Cambridge University Press, Cambridge, 1997); D.N. Schramm and M.S. Turner, Rev. Mod. Phys. **70**, 303 (1988).
- [2] A.M. Boesgaard and G. Steigman, Ann. Rev. Astron. Astrophys. **23**, 319 (1985).
- [3] T.P. Walker, G. Steigman, D.N. Schramm, K.A. Olive, and H.-S. Kang, Ap. J. **376**, 51 (1991).
- [4] M.S. Smith, L.H. Kawano, and R.A. Malaney, Ap. J. **85**, 219 (1993).
- [5] C.J. Copi, D.N. Schramm, and M.S. Turner, Phys. Rev. Lett. **75**, 3981 (1995).
- [6] P.J. Kernan and L.M. Krauss, Phys. Rev. Lett. **72**, 3309 (1994).
- [7] F.W. Stecker, Phys. Rev. Lett. **44**, 1237 (1980); K.A. Olive and M.S. Turner, Phys. Rev. Lett. **46**, 516 (1981); S.P. Riley and J.M. Irvine, J. Phys. G **17**, 35 (1991); G.M. Fuller, R.N. Boyd, and J.D. Kalen, Ap. J. **371**, L11 (1991); K.A. Olive, G. Steigman, and T.P. Walker, Ap. J. **380**, L1 (1991).
- [8] D.A. Dicus, E.W. Kolb, A.M. Gleeson, E.C.G. Sudarshan, V.G. Teplitz, and M.S. Turner, Phys. Rev. D **26**, 2694 (1982).
- [9] K.A. Olive, G. Steigman, and E.D. Skillman, Ap. J. **483**, 788 (1997).
- [10] J.L. Linsky *et al.*, Ap. J. **402**, 694 (1993).
- [11] G. Steigman and M. Tosi, Ap. J. **401**, 150 (1992); N. Hata, R.J. Scherrer, G. Steigman, D. Thomas, and T.P. Walker, Ap. J. **458**, 637 (1996); G. Steigman and M. Tosi, Ap. J. **453**, 173 (1995); M. Tosi, G. Steigman, F. Matteucci, and C. Chiappini, Ap. J. **498**, 226 (1998).
- [12] N. Hata, R.J. Scherrer, G. Steigman, D. Thomas, T.P. Walker, S. Bludman, and P. Langacker, Phys. Rev. Lett. **75**, 3977 (1995).
- [13] B.D. Fields, K. Kainulainen, K.A. Olive, and D. Thomas, New Astronomy **1**, 77 (1996).
- [14] S.T. Scully, M. Cassé, K.A. Olive, D.N. Schramm, J. Truran, and E. Vangioni-Flam, Ap. J. **462**, 960 (1996); S. Scully, M. Cassé, K.A. Olive, and E. Vangioni-Flam, Ap. J. **476**, 521 (1997); D. Galli, L. Stanghellini, M. Tosi, and F. Palla, Ap. J. **477**, 218 (1997).
- [15] P.J. Kernan and S. Sarkar, Phys. Rev. D **54**, R3681 (1996).
- [16] D. Sasselov and D. Goldwirth, Ap. J. **444**, L5 (1995); G. Steigman, S.M. Viegas, and R. Gruenwald, Ap. J. **490**, 187 (1997).
- [17] Yu.I. Izotov and T.X. Thuan, Ap. J. **497**, 227 (1998); Yu.I. Izotov and T.X. Thuan, Astrophys. J., in press (1998).
- [18] E. Terlevich, talk given at “Synthesis of Light Nuclei in the Early Universe”, ECT*, Trento, Italy, June 1997.

[19] M. Kawasaki, P. Kernan, Ho-Shik Kang, R.J. Scherrer, G. Steigman, and T.P. Walker, *Nucl. Phys.* **B419**, 105 (1994); M. Kawasaki, K. Kohri, and K. Sato, astro-ph/9705148.

[20] The Super-Kamiokande Collaboration, hep-ex/9805006

[21] K. Enqvist, K. Kainulainen, and M. Thomson, *Nucl. Phys.* **B373**, 498 (1992); *Phys. Lett.* **B288**, 145 (1992).

[22] N. Terasawa and K. Sato, *Phys. Lett.* **B185**, 412 (1987); K. Enqvist, K. Kainulainen, and M. Thomson, *Phys. Rev. Lett.* **B373**, 498 (1992).

[23] S. Dodelson, G. Gyuk, and M.S. Turner, *Phys. Rev. D* **40**, 5068 (1994).

[24] S. Hannestad, *Phys. Rev. D* **57**, 2213 (1998).

[25] D.S. Balser, T.M. Bania, C.J. Brockway, R.T. Rood, and T.L. Wilson, *Ap. J.* **430**, 667 (1994); G. Gloeckler and J. Geiss, *Nature* **381**, 210 (1996); M.S. Turner, J.W. Truran, D.N. Schramm, and C.J. Copi, *Ap. J.* **466**, L59 (1996); D.S. Balser, T.M. Bania, R.T. Rood, and T.L. Wilson, *Ap. J.* **483**, 320 (1997).

[26] F. Spite and M. Spite, *Astron. Astrophys.* **115**, 357 (1982); *Nature* **297**, 483 (1992); M. Spite, P. François, P.E. Nissen, and F. Spite, *Astron. Astrophys.* **307**, 172 (1996).

[27] P. Bonifacio, and P. Molaro, *Mon. Not. R. Astr. Soc.*, **285**, 847 (1997).

[28] M.H. Pinsonneault, T.P. Walker, G. Steigman, and V.K. Narayanan, astro-ph/9803073.

[29] S. Vauclair and C. Charbonnel, astro-ph/9802315.

[30] A. Songaila, L.L. Cowie, C.J. Hogan, and M. Rugers, *Nature* **368**, 599 (1994); R.F. Carswell, M. Rauch, R.J. Weymann, A.J. Cooke, and J.K. Webb, *Mon. Not. R. Astr. Soc.*, **268**, L1 (1994); M. Rugers and C.J. Hogan, *Ap. J.* **459**, L1 (1996); D. Tytler, X.-M. Fan, and S. Burles, *Nature* **381**, 207 (1996); S. Burles and D. Tytler, astro-ph/9603070; D. Tytler, S. Burles, and D. Kirkman, astro-ph/9612121.

[31] S. Burles and D. Tytler, astro-ph/9803071.

[32] A. Songaila, E.J. Wampler, and L.L. Cowie, *Nature* **385**, 137 (1997); A. Songaila, astro-ph/9709293; S. Burles and D. Tytler, *Astron. J.* **114**, 1330 (1997); S.A. Levshakov, W.H. Kegel, and F. Takahara, *Ap. J.* **499**, L1 (1998).

[33] J.K. Webb, R.F. Carswell, K.M. Lanzetta, R. Ferlet, M. Lemoine, A. Vidal-Madjar, and D.V. Bowen, *Nature* **388**, 250 (1997); astro-ph/9710089.

[34] G. Steigman, N. Hata, and J.E. Felten, astro-ph/9708016.

[35] J.H. Applegate, C.J. Hogan, and R.J. Scherrer, *Phys. Rev. D* **35**, 1151 (1987).

[36] C. Alcock, G.M. Fuller, and G.J. Mathews, *Ap. J.* **320**, 439 (1987); G.M. Fuller, G.J. Mathews, and C.R. Alcock, *Phys. Rev. D* **37**, 1380 (1988).

[37] R.M. Malaney and W.A. Fowler, *Ap. J.* **333**, 14 (1988).

[38] H. Kurki-Suonio, R.A. Matzner, J.M. Centrella, T. Rothman, and J.R. Wilson, *Phys. Rev. D* **38**, 1091 (1988); H. Kurki-Suonio and R.A. Matzner, *Phys. Rev. D* **39**, 1046 (1989).

[39] N. Terasawa and K. Sato, *Phys. Rev. D* **39**, 2893 (1989).

[40] H. Kurki-Suonio, R.A. Matzner, K.A. Olive, and D.N. Schramm, *Ap. J.* **353**, 406 (1990).

[41] C.R. Alcock, D.S. Dearborn, G.M. Fuller, G.J. Mathews, and B.S. Meyer, *Phys. Rev. Lett.* **64**, 2607 (1990).

[42] G.J. Mathews, B.S. Meyer, C.R. Alcock, and G.M. Fuller, *Ap. J.* **358**, 36 (1990).

[43] H. Kurki-Suonio and R.A. Matzner, *Phys. Rev. D* **42**, 1047 (1990).

[44] B.S. Meyer, C.R. Alcock, G.J. Mathews, and G.M. Fuller, *Phys. Rev. D* **43**, 1079 (1991).

[45] D. Thomas, D.N. Schramm, K.A. Olive, G.J. Mathews, B.S. Meyer, and B.D. Fields, *Ap. J.* **430**, 291 (1994).

[46] K. Jedamzik, G.M. Fuller, and G.J. Mathews, *Ap. J.* **423**, 50 (1994).

[47] G.J. Mathews, T. Kajino, and M. Orito, *Ap. J.* **456**, 98 (1996); M. Orito, T. Kajino, R.N. Boyd, and G.J. Mathews, *Ap. J.* **488**, 515 (1997).

[48] E. Witten, *Phys. Rev. D* **30**, 272 (1984).

[49] J.H. Applegate and C.J. Hogan, *Phys. Rev. D* **31**, 3037 (1985).

[50] H. Kurki-Suonio, *Phys. Rev. D* **37**, 2104 (1988).

[51] J. Ignatius, K. Kajantie, H. Kurki-Suonio, and M. Laine, *Phys. Rev. D* **50**, 3738 (1994).

[52] M.B. Christiansen and J. Madsen, *Phys. Rev. D* **53**, 5446 (1996).

[53] V. Rubakov and M.E. Shaposhnikov, *Phys. Usp.* **39**, 461 (1996).

[54] D. Comelli, M. Pietroni, A. Riotto, *Phys. Rev. D* **50**, 7703 (1994).

[55] M. Giovannini and M.E. Shaposhnikov, *Phys. Rev. Lett.* **80**, 22 (1998); *Phys. Rev. D* **57**, 2186 (1998).

[56] J.B. Rehm and K. Jedamzik, astro-ph/9802255.

[57] H. Kurki-Suonio and E. Sihvola, in progress.

[58] A.E. Nelson, D.B. Kaplan, and A.G. Cohen, *Nucl. Phys. B* **373**, 453 (1991).

[59] G.R. Farrar and M.E. Shaposhnikov *Phys. Rev. D* **50**, 774 (1994).

[60] J.M. Cline, K. Kainulainen, and A. Visher, *Phys. Rev. D* **54**, 2451 (1996).

[61] A.F. Heckler, *Phys. Rev. D* **51**, 405 (1995).

[62] M. Joyce, T. Prokopec, and N. Turok, *Phys. Rev. D* **53**, 2958 (1996).

[63] J.M. Cline, M. Joyce, and K. Kainulainen, *Phys. Lett. B* **417**, 79 (1998).

[64] J. Cline, M. Joyce, and K. Kainulainen, in progress.

[65] G.D. Moore and T. Prokopec, *Phys. Rev. D* **52**, 7182 (1995).

[66] H. Kurki-Suonio and M. Laine, *Phys. Rev. Lett.* **77**, 3951 (1996).

[67] G.M. Fuller, K. Jedamzik, G.J. Mathews, and A. Olinto, *Phys. Lett. B* **333**, 135 (1994).

[68] M. Laine and K. Rummukainen, hep-lat/9804019, hep-ph/9804255.

[69] R.E. Leonard and R.J. Scherrer, *Ap. J.* **463**, 420 (1996).

[70] Y. Iwasaki *et al.* (QCDPAX Collaboration), *Phys. Rev. D* **46**, 4657 (1992); B. Grossmann and M. L. Laursen, *Nucl. Phys. B* **408**, 637 (1993); Y. Iwasaki, K. Kanaya, L. Kärkkäinen, K. Rummukainen, and T. Yoshié, *Phys. Rev. D* **49**, 3540 (1994).

[71] R. Lopez, M. Turner, and G. Gyuk, work in progress.

[72] K. Jedamzik and G.M. Fuller, *Ap. J.* **423**, 33 (1994).